1 **Engineering butylglyceryl-modified polysaccharides towards nanomedicines for brain**
2 **drug delivery**

3 Mohammad F. Bostanudin[a,b], Aikaterini Lalatsa[b], Dariusz C. Górecki[b], Eugen Barbu[b,*]

4 [a]College of Pharmacy, Al Ain University, Abu Dhabi 112612, UAE
5 [b]School of Pharmacy and Biomedical Sciences, University of Portsmouth, St Michael's
6 Building, White Swan Road, PO1 2DT, United Kingdom
7
8

9 **Abstract**

10 Colloidal systems prepared from carbohydrates are subject of intense research due to their
11 potential to enhance drug permeability through biological membranes, however their
12 characteristics and performance are never compared directly. Here we report the results of a
13 comparative investigation of a series of butylglyceryl-modified polysaccharides (chitosan, guar
14 gum, and pullulan) that were formulated into nanoparticles and loaded with a range of model
15 actives (Doxorubicin, Rhodamine B, Angiotensin II). Butylglyceryl-modified guar gum and
16 corresponding pullulan nanocarriers were more stable at physiological pH compared to those
17 obtained from modified chitosan, and studies of the in-vitro interactions with mouse brain
18 endothelial cells (bEnd3) indicated an increased biological membrane permeability and lack of
19 toxicity at application-relevant concentrations. No significant haemolytic effect was observed,
20 and confocal microscopy and flow cytometry studies confirmed the efficient cellular uptake
21 and cytoplasmic localisation of NPs. Most promising characteristics for brain drug delivery
22 applications were demonstrated by butylglyceryl pullulan nanocarriers.
23
24

25 **Keywords:** nanoparticles; pullulan; guar gum; chitosan; polysaccharides; drug delivery;
26 brain.
27
28

29 **1. Introduction**

30 A significant number of brain disorders are considered responsible for the rising
31 morbidity and mortality observed in both developed and developing countries (Raggi &
32 Leonardi, 2019), but real progress in the treatment of many neurological disorders has been
33 long hindered by the inability of most drugs to enter the brain – despite recent technological
34 advances, the blood-brain barrier (BBB) continues to represent a major challenge (Aikaterini

This is a peer-reviewed, accepted author manuscript of the following article: Bostanudin, M. F., Lalatsa, A., Górecki, D. C., & Barbu, E. (2020). Engineering butylglyceryl-modified polysaccharides towards nanomedicines for brain drug delivery. Carbohydrate Polymers, 236, [116060]. https://doi.org/10.1016/j.carbpol.2020.116060

35 Lalatsa & Barbu, 2016). In concerted efforts to enhance drug concentration in the brain, many
36 strategies have been considered, however it has been found that the benefits registered with
37 several invasive methods come at the rather high cost of harmful side effects (Aikaterini
38 Lalatsa, Schatzlein, & Uchegbu, 2014). Current research tends therefore to concentrate on non-
39 invasive strategies, with the use of colloidal drug carriers as a most promising approach for
40 systemic brain delivery (Godfrey et al., 2018; Lu et al., 2014).

41 Among the carbohydrates investigated, of particular interest are polysaccharides: they
42 are highly stable, non-toxic, biodegradable, possess hydrophilic moieties that mediate non-
43 covalent interactions with biological tissues (Hervé, Ghinea, & Scherrmann, 2008), and can be
44 converted into amphiphilic materials that self-assemble into colloidal carriers (Bostanudin,
45 Arafat, Sarfraz, Górecki, & Barbu, 2019; A. Lalatsa et al., 2015; Toman et al., 2015). Due to
46 its low cost, widespread availability and ease of chemical modification, chitosan (CS) has been
47 one of the most intensively studied polysaccharides for brain drug delivery applications,
48 demonstrating indeed very promising results (A. Lalatsa et al., 2015; Lien et al., 2012; Toman
49 et al., 2015). Rationalised by the ability of short chain alkylglycerols to enhance drug access
50 into the brain *in vivo* when administered intracarotidally (Erdlenbruch et al., 2003), dextran
51 and chitosan have been previously modified with alkylglycerols and formulated into
52 nanoparticles, which were shown to be taken up by endothelial brain cells and to increase drug
53 permeability *in vitro* and *in vivo* (Boussahel et al., 2017; Ibegbu, Boussahel, Cragg, Tsibouklis,
54 & Barbu, 2017; Lien et al., 2012; Molnár, Barbu, Lien, Górecki, & Tsibouklis, 2010; Toman
55 et al., 2015). In contrast to chitosan, polysaccharides of similar generic features but lacking a
56 ionisable amino group that can negatively impact on the nanomedicines' colloidal stability,
57 such as pullulan (PUL) and guar gum (GG), have been less investigated for their potential in
58 similar drug delivery applications (Singh, Kaur, Rana, & Kennedy, 2017). Also, to our
59 knowledge, no comparative investigations into the characteristics and *in vitro* performance
60 (such as drug loading, brain cells uptake and permeability) of different polysaccharides have
61 been reported.

62 Investigating the hypothesis that nanomedicines based on amphiphilic pullulan and
63 guar gum can provide improved characteristics relevant to brain drug delivery applications
64 compared to similarly-modified chitosan-based materials, we describe here the preparation and
65 characterisation of colloidal formulations obtained from novel butylglyceryl-modified PUL
66 and GG and loaded with a range of model actives (Doxorubicin, Rhodamine B, Angiotensin
67 II). Results of *in vitro* investigations comparing the interactions of these nanocarriers with
68 mouse brain endothelial cells (bEnd3) in terms of cytotoxicity, cellular uptake and BBB model

69 membrane permeability, relative to butylglyceryl-modified CS nanoparticles, are also
70 presented.
71

72 **2. Materials and methods**

73 *2.1. Materials*

74 Low molecular weight (MW) chitosan (MW 50–190 kDa; 75-85% deacetylation; cat.
75 no. 448869; batch no. MKBD0020), pullulan (MW 100 kDa; cat. no. 91335; batch no.
76 BCBK3803V), guar gum (MW 220 kDa; cat. no. G4129; batch no. 041M0058V),
77 dimethylformamide (DMF; anhydrous, 99.8%), dimethyl sulfoxide (DMSO; anhydrous, ≥
78 99.9%), nbutylglycidyl ether (BGE; reagent grade 95%), potassium *tert*-butoxide (t-BuOK;
79 reagent grade > 97%), phthalic anhydride (reagent grade ≥ 99.9%), sodium tripolyphosphate
80 (TPP), sodium hydroxide (NaOH), Span 80, glycerol (reagent grade ≥ 99.5%), glutaraldehyde
81 (25% in H_2O; cat. no. G6257), Rhodamine B base (Dye content 97%), Angiotensin II human
82 (HPLC grade ≥ 93%), Triton X-100, Hydrocortisone (HPLC grade ≥ 98%), Adenosine 3',5'-
83 Cyclic Monophosphate (HPLC grade ≥ 98.5%) and Fluorescein Isothiocyanate (FITC) labelled
84 dextran (MW 500 kDa) were sourced from Sigma Aldrich (Gillingham, UK).
85 Hydrazine monohydrate, acetic acid, dimethylsulfoxide (DMSO, analytical grade), and
86 dichloromethane (DCM) were purchased from Fisher Scientific (Loughborough, UK).
87 Doxorubicin was obtained from Carbosynth (Compton, UK). Texas Red-X succinimidyl ester
88 (mixed isomers), Texas Red-X dichlorotriazine, Dulbecco's Modified Eagle Medium (DMEM)
89 media, NucGreen Dead 488 and TrypLE Express were sourced from Life Technologies Ltd.
90 (Paisley, UK). Phosphate Buffered Saline (PBS) was purchased from Gibco (Paisley, UK).
91 Forskolin and RO-20-1724 were obtained from Enzo Life Sciences (Exeter, UK).
92

93 *2.2. Synthesis and characterisation of butylglyceryl-modified polysaccharides*

94 The synthesis was adapted from methods described in the literature (Bostanudin et al.,
95 2019; Molnár et al., 2010), with some modifications. Briefly, an alkaline solution of
96 polysaccharide (either 2.78 mmol GG, 3.05 mmol PUL or 4.39 mmol phthaloylated CS,
97 dissolved in either water, DMSO, or DMF, respectively) was reacted with *n*-butylglycidyl ether
98 in different ratios (3–114 mmol, *Figure 1)*. The reaction mixture was left stirring overnight
99 then purified by washing (x3) with DCM and/or dialysis (MWCO 3.5 kDa, Medicell Ltd,
100 London, UK) against deionised water (10 L; 9 changes over 72 h) prior to lyophilisation. All

101 materials were characterised by ^{1}H-NMR spectroscopy using a JEOL Eclipse 400+ instrument
102 (JEOL, Welwyn Garden City, UK; 400 MHz) and the degree of substitution (DS) was
103 calculated from the ^{1}H-NMR spectra. FT-IR spectra were recorded on a Nexus Euro infrared
104 spectrometer (Thermo Fisher Scientific, Hemel Hempstead, UK) and Gel permeation
105 chromatography (GPC) was performed using a Waters Alliance GPC 2000 system (Waters
106 Corporation, Milford, MA, USA) (details in the *Supplementary Materials*)
107

108 *2.3. Formulation of butylglyceryl-modified guar gum nanoparticles*

109 Span 80 (0.4 g) solution in DCM (3.33 mL) was added to a butylglyceryl-modified GG;
110 GG-OX4 solution (10 mL) of specific concentration (0.5–2% w/v; different DS) under stirring.
111 Glycerol (1 mL) was added, followed by glutaraldehyde (1 mL; 3% v/v) under stirring and was
112 left stirring overnight prior to ultracentrifugation (x3 ultracentrifuge; Beckman Coulter, High
113 Wycombe, UK; 70.1 Ti rotor; 164,391 g; 30 min); the pellet was washed three times with
114 deionised water and freeze-dried, affording nanoparticles as white powder (55–65% yield).

115 *2.4. Formulation of butylglyceryl-modified pullulan nanoparticles*

116 Butylglyceryl-modified PUL solution; PUL-OX4 in DMSO (2 mL) at varying
117 concentrations (1–10 mg/mL; different DS) was added to ultrapure water (8 mL) under stirring.
118 The nanoparticles were dialysed (MWCO 12-14 kDa, Medicell Ltd, London, UK) against
119 deionised water (10 L; 9 changes over 72 h) and lyophilised, affording nanoparticles as beige
120 powder (yields 76–83%).

121 *2.5. Formulation of butylglyceryl-modified chitosan nanoparticles*

122 Sodium tripolyphosphate (2 mL) aq. solution at varying concentrations (0.1–0.3
123 mg/mL) was introduced dropwise (1 mL/min) under stirring to butylglyceryl-modified chitosan
124 solution; CS-OX4 (1.07–2.5 mg/mL; various DS) in aq. acetic acid (1% v/v, 6 mL). The
125 nanoparticles were ultracentrifuged (164,391 g; 30 min), washed (x3) with deionised water,
126 and lyophilised, affording nanoparticles as beige powder (yields 16–45%).

127 *2.6. Morphological characterisation*

128 The nanoparticles diameter was determined by dynamic light scattering (DLS) using a
129 Malvern ZetasizerNano ZS instrument equipped with a 633 nm He-Ne laser (173° scattering
130 angle) (Malvern Instruments Ltd., Worcestershire, UK), calibrated by 100–400 nm polystyrene

131 latex standard beads and DTS 1050 latex beads (Malvern Instruments Ltd). Samples were
132 analysed (x3) at 25 °C and the results were expressed as Z-average mean and polydispersity
133 index (PDI). Electrophoretic mobility measurements were conducted using the same
134 instrument to determine the ZP. Investigation on nanoparticles stability at varying pH values
135 (3–8.5) was performed employing a Multi-Purpose Titrator-2 instrument (Malvern Instruments
136 Ltd.). The nanoparticles were redispersed (0.5 mg/mL) in an ultrapure water and the pH was
137 adjusted with NaOH solution (0.005 M), and HCl (0.05 M); the diameter and ZP were
138 measured at 0.5 pH increments. Complementary size determination was conducted using a
139 Nanoparticle Tracking Analysis (NTA) LM-14 instrument (Malvern Instruments Ltd.)
140 equipped with a 532 nm green laser at 25 °C.

141 Scanning Electron Microscopy (SEM) was performed by depositing aqueous
142 nanoparticles dispersion (5 mg/mL) onto a metallic stub prior to coating with Au/Pd under
143 argon using a Q150RES sputter coater (Quorum Technologies Ltd., Ashford, UK), and imaged
144 using a JEOL-JSM-6060LV SEM Microscope (JEOL). For Transmission Electron Microscopy
145 (TEM), aq. dispersion (5 mg/mL) was placed onto the TEM copper grid surface (3.0 mm, 200
146 mesh, coated with Formvar film), stained with 2% (w/v) uranyl acetate staining solution and
147 imaged with a JEOL JEM 2100 TEM Microscope (JEOL).

148 *2.7. Model actives loading and release studies*

149 A solution of either Rhodamine B (0.5 mL; 0.037 mg/mL in DMSO), Doxorubicin (0.5
150 mL; 0.4 mg/mL in DMSO) and Angiotensin II (1 mL; 0.1 mg/mL in deionised water) were
151 mixed with polymer solution during nanoparticles preparation *via* various techniques (section
152 2.3−2.5). The nanoparticles were ultracentrifuged (164,391 g; 30 min); the pellets were
153 lyophilised and weighed; the supernatant was measured for the unbound model actives amount
154 by UV/Vis spectroscopy measurements employing a Lambda 650 Ultra Violet/Visible
155 Spectrometer (Perkin Elmer, Buckinghamshire, UK; measuring at 544 nm for Rhodamine B;
156 486 nm for Doxorubicin). For Angiotensin II detection, HPLC analysis was performed using
157 an Agilent 1100 series HPLC system (Agilent Technologies, Waldbron, Germany; C18
158 reversed phase column; acetonitrile/trifluoroacetic acid (TFA) 99.9:0.1 v/v, linear gradient
159 10−60% (0.7 ml/min); retention time = 8.32 min; lower detection limit = 25 ng/mL. The drug
160 loading was calculated using Equation (2):

161

162 $$DL\ (\%) = \frac{weight\ of\ drug}{weight\ of\ nanoparticles}\ x\ 100 \quad (2)$$

163 For the release studies, nanoparticles were re-dispersed (1.5 mg/mL) in PBS (pH 7.4;
164 saline 0.9%), aliquots (1.5 mL) were taken and distributed into Eppendorf tubes, which were
165 then placed in a thermostatic (37 °C) shaking water bath. At varying time points, an aliquot
166 (700 μL) was individually removed from the supernatant and analysed using either HPLC or
167 UV/Vis.

168 *2.8. Nanoparticles fluorescent labelling*

169 A Texas Red-X dichlorotriazine solution in DMSO (0.5 mL; 2 mg/mL) was added to
170 either GG-OX4 in 0.1 M sodium bicarbonate buffer (10 mL; 10 mg/mL) or PUL-OX4 solution
171 in DMSO/0.1 M sodium bicarbonate buffer (70:30 v/v; 10 mL; 10 mg/mL) under stirring. CS-
172 OX4 labelling was performed employing Texas Red-X succinimidyl mixed ester in DMSO
173 (0.5 mL; 2 mg/mL), where it was added to the polymer dispersion in 0.1 M sodium bicarbonate
174 buffer (10 mL; 10 mg/mL) under stirring; maintained for 1 h. Labelled GG-OX4 and PUL-
175 OX4 was precipitated with DCM, centrifuged (2,880 g; 30 min) using a Jouan B4i (Thermo
176 Fisher Scientific), purified by either washing (x3) with DMSO for labelled CS-OX4 or dialysis
177 (MWCO 12-14 kDa) against deionised water (10 L; 3 exchanges over 24 h) for labelled GG-
178 OX4 and PUL-OX4 and then lyophilised, affording Texas Red-labelled polymer; GG-OX4 as
179 a purple and fluffy cotton-like material (yields 78– 81%), PUL-OX4 and CS-OX4 as a purple
180 powder (yields 71–73% and 71–75% respectively). The degree of labelling was analysed by
181 UV/Vis spectroscopy (measuring at 589 nm) and calculated using Equation (3):

182 $$Degree\ of\ labelling\ (\%) = \frac{weight\ of\ Texas\ Red}{weight\ of\ nanoparticles} \times 100 \quad (3)$$

183 *2.9. Cell culture*

184 Mouse brain endothelial (bEnd3) cells were obtained from the European Collection of
185 Cell Cultures (ECACC). The cells (passage no. 37–45) were cultured in a modified DMEM
186 media, enriched with supplements (*Table S1, Supplementary Materials*). The cells were grown
187 at 37°C with 5% CO_2 under humidified atmosphere in an incubator. Trypsinisation was
188 performed with TrypLE Express and flasks were equilibrated at 37°C for 10–15 min. The cell
189 suspension was harvested (115 g; 5 min) using a Beoco C28A (Wolf Laboratories, Pocklington,
190 UK) for further use.

191 *2.10. Cytotoxicity assays*

192 Nanoparticles (50 μL; dispersed in modified DMEM at concentrations 1–10 mg/mL)
193 were incubated with confluent bEnd3 cells (seeding 4.0 x 10^4). Sterile PBS and Triton-X (0.1%
194 v/v) were used as negative and positive controls respectively. After 24 h incubation, media was
195 replaced with MTT solution (100 μL, 1 mg/mL) and incubated (37ºC) for another 1 h prior to
196 be replaced by DMSO (100 μL) and analysed using a POLARstar OPTIMA (BMG Labtech,
197 Aylesbury, Bucks, UK; measuring at 570 nm).

198 *2.11. Confocal microscopy analysis*

199 Nanoparticle suspension in modified DMEM (2 mL; 0.5 mg/mL) were incubated with
200 confluent bEnd3 cells (seeding 4.0 x 10^4) for 3 h; cells without nanoparticles were used as a
201 control. The cells were washed (x3) with PBS, fixed in paraformaldehyde (4% w/v; 4ºC) and
202 permeabilised with Tween 20 (0.1% v/v) prior to 15 min incubation with NucGreen Dead 488
203 before visualisation using a confocal microscope (LSM 510 META, ZEISS, Carl Zeiss,
204 Oberkochen, Germany; 488 nm for NucGreen and 543 nm for Texas Red).

205 *2.12. Flow cytometry analysis*

206 Doxorubicin-loaded nanoparticles (2 mL; 0.5 mg/mL in modified DMEM) were
207 incubated with confluent bEnd3 cells (seeding 4.0 x 10^4) for 3 h. The cells were harvested (115
208 g; 5 min) and redispersed in PBS (400 μL) for analysis. Cells treated with propidium iodide
209 (1% v/v; without nanoparticles) were used as a control. Flow cytometry was performed on a
210 four-colour multi parameter BD FACSCalibur system (BD Biosciences, Oxford, UK) equipped
211 with a 488 nm argon gas laser and a 635 nm red-diode laser; Doxorubicin emission
212 fluorescence was measured using a 530/30 nm filter.

213 *2.13. Fluorescent marker translocation across bEnd3 cell monolayers studies*

214 bEnd3 cells were seeded (4 x 10^4 cells) in a Transwell-type BBB model comprising of
215 a sterile 24-well plate Millipore Millicell; incubated at 37ºC until confluent. A specific cocktail
216 (consisting of cAMP (250 μM), RO-20-1724 (20 μM), Forskolin (50 μM) and hydrocortisone
217 (550 μM)) was applied and incubation continued for another 24 h. Nanoparticles (2 mg/mL)
218 and FITC-dextran (100 μg/mL) dispersed in media were simultaneously applied to each well
219 and the FITC-dextran concentration in the basolateral compartment was then monitored;
220 samples (100 μL) were collected every 30 min (for 3 h) for analysis using a POLARstar
221 OPTIMA fluorescence plate reader (BMG Labtech) (485 nm/520 nm excitation/emission

222 wavelengths). The apparent permeability coefficient (Papp) was calculated based on Equation
223 (4):

224 $$Papp\ (cm.s^{-1}) = \frac{dQ}{dt} \times \frac{V_R}{A \times Co \times 60} \quad (4)$$

225 where;

226 dQ/dt FITC-dextran flux transported across the membrane (µg/sec)

227 V_R basolateral volume (600 µL)

228 A filter insert surface area (0.33 cm^2)

229 Co FITC-dextran initial mass concentration at the apical side (100 µg/mL)

230 60 conversion factor (min to s)

231

232 *2.14. Haemolysis studies*

233 Blood was obtained from a male Wistar rat (450 g), after CO_2 asphyxiation, by
234 collection from the heart using a 21G needle into a BD Vacutainer tube (lithium heparin) and
235 kept on ice. The red blood cells (RBC) were separated by centrifugation (Heraeus Multifuge
236 3SR Plus; 2000 g; 10 min; 4ºC); the plasma fraction was removed before washing the RBC
237 with PBS (x3) and centrifuged (2,000 g; 10 min), before dilution with PBS (4% w/v) to yield
238 a cell suspension. PBS and Triton-X (1% v/v) were used as negative and positive controls
239 respectively. NPs suspensions were added (10 µL) to RBC cell suspension (190 µL) and then
240 incubated (37 ºC) for 1 h prior to centrifugation (1200 g; 10 min; 4ºC); the supernatant (150
241 µL) absorbance was measured at 570 nm using a Multiskan GO microplate reader (Thermo
242 Fisher Scientific). Haemolysis percentage was calculated using Equation (5):

243 $$Haemolysis\ (\%) = \frac{Sample_{Absorbance} - negative\ control_{Absorbance}}{Positive\ control_{Absorbance} - negative\ control_{Absorbance}} \times 100 \quad (5)$$

244

245 *2.15. Data statistical analysis*

246 Statistical analysis was performed using SPSS Statistics v.22 software (SPSS Inc.,
247 Chicago, IL, USA, 2013). Results were expressed as mean ± standard deviation (SD) values;
248 significance was tested using analysis of variance (ANOVA), p values were set at 0.05, unless
249 stated otherwise.

250

3. Results and discussion

Butylglyceryl-modified polysaccharides were synthesised *via* a nucleophilic substitution reaction using *n*-butylglycidyl ether (*Figure 1*) as follow: GG-OX4 synthesis was achieved under strong alkaline conditions (aq. NaOH, pH 14); PUL-OX4 preparation was performed in DMSO with t-BuOK as a base; and CS-OX4 has been prepared by protecting the free amino groups with phthaloyl moieties, followed by butylglyceryl pendant chain attachment to the available polysaccharidic hydroxyl groups and phtahloyl groups removal using hydrazine (Molnár et al., 2010). Their structures were confirmed by FT-IR and ^{1}H-NMR spectroscopy, with molecular weight between 100kDa and 300kDa as measured by GPC (*Figures S1–S3, Supplementary Materials)*.

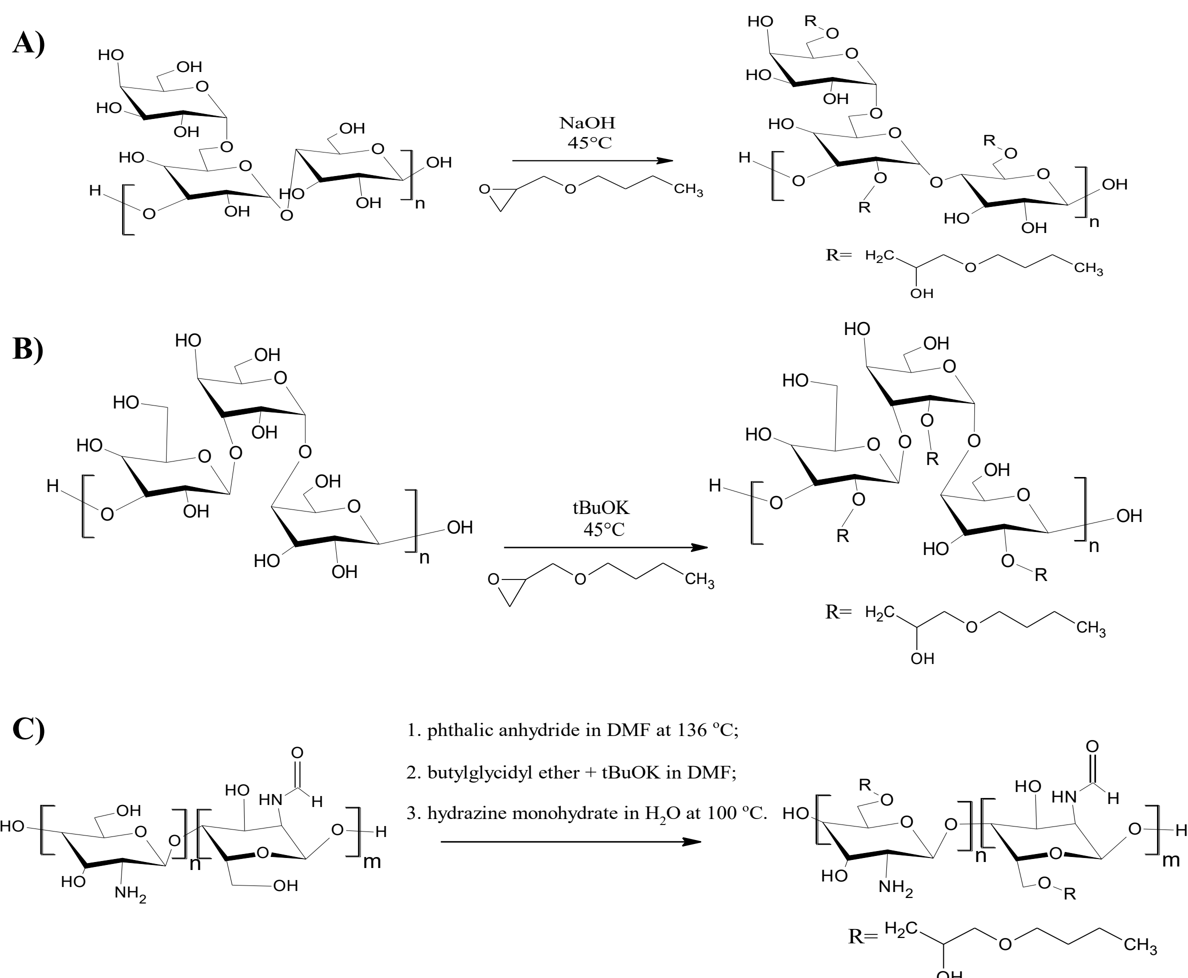

Figure 1. Schematic synthesis of: A) GG-OX4, B) PUL-OX4, and C) CS-OX4.

GG-OX4, CS-OX4, and PUL-OX4 derivatives with different degree of substitution (DS) have been formulated into nanoparticles with characteristics summarised in Table 1. The

270 size of nanoparticles was found to increase very slightly with concentration, possibly an effect
271 due to a corresponding increase in viscosity (Chen, Mohanraj, Wang, & Benson, 2007).
272 Reverse emulsification was employed to formulate GG-OX4 nanoparticles using
273 glutaraldehyde as a cross-linker. Results *(Table 1)* indicate that GG-OX4 with lower DS values
274 (DS 3.6, 12.6 and 33.9%) produced nanoparticles (yields 57–67%) with size in the range of
275 145–200 nm, with good PDI (ca. 0.2) and negative ZP values (-22 to -33 mV). PUL-OX4
276 nanoparticles with different DS and concentrations were prepared by nanoprecipitation, when
277 nanoparticles around 120–180 nm, with good PDI (ca. 0.2) and negative ZP values (-23 to -32
278 mV) were obtained. CS-OX4 nanoparticles were prepared by ionotropic gelation with TPP,
279 and results suggest that the yields increased with the TPP concentration (optimum 0.2 mg/mL),
280 yielding nanoparticles (yields ~33%) with size around 145 (measured by DLS and NTA),
281 monodispersed (PDI=0.32) and positive ZP value (34.1 mV). The ZP was found to decrease
282 with an increase in the TPP concentration, likely because of the negatively charged TPP.
283

284 *Table 1. Characteristics of nanoparticles at varying concentrations and DS (n=3; ±SD).*

Material	DS (%)	Polymer conc. (% w/v)	TPP conc. (mg/mL)	Diameter NTA (nm)	Diameter DLS (nm)	Polydispersity Index	Zeta Potential (mV)	Yield (% w)
GG-OX4	3.6	0.5	N/A	145 ± 12	169 ± 9	0.22 ± 0.02	-32.7 ± 5.2	67 ± 5
		1.0		157 ± 15	17 ± 7	0.19 ± 0.02	-28.8 ± 2.9	57 ±15
		2.0		172 ± 16	200 ± 11	0.29 ± 0.03	-27.1 ± 7.0	58 ± 13
	12.6	0.5		166 ± 11	166 ± 3	0.21 ± 0.09	-29.9 ± 4.6	60 ± 10
		1.0		167 ± 13	170 ± 5	0.18 ± 0.06	-23.8 ± 1.9	58 ± 8
		2.0		178 ± 9	186 ± 8	0.15 ± 0.11	-22.1 ± 3.0	62 ± 9
	33.9	0.5		167 ± 11	167 ± 4	0.24 ± 0.04	-32.4 ± 6.2	61 ± 10
		1.0		176 ± 11	177.0 ± 11	0.20 ± 0.09	-25.5 ± 2.9	66 ± 11
		2.0		189 ± 17	192 ± 6	0.17 ± 0.10	-30.1 ± 5.7	59 ± 9
PUL-OX4	47.0	1	N/A	139 ± 22	143 ± 12	0.20 ± 0.10	-29.2 ± 2.8	79 ± 5
		5		157 ± 20	155 ± 6	0.18 ± 0.07	-27.9 ± 1.7	80 ± 4
		10		177 ± 17	182 ± 8	0.14 ± 0.06	-29.9 ± 1.4	81 ± 4
	58.5	1		133 ± 16	136 ± 15	0.21 ± 0.08	-23.4 ± 1.9	76 ± 5
		5		141 ± 12	145 ± 9	0.19 ± 0.11	-28.2 ± 3.3	77 ± 7
		10		158 ± 18	163 ± 8	0.17 ± 0.02	-30.1 ± 5.2	76 ± 9
	77.3	1		124 ± 23	125 ± 13	0.18 ± 0.12	-29.0 ± 4.3	82 ± 7
		5		132 ± 19	142± 12	0.17 ± 0.09	-31.9 ± 5.1	83 ± 5
		10		141 ± 20	178 ± 9	0.21 ± 0.05	-29.8 ± 2.9	79 ± 9
CS-OX4	14.1	1.07	0.10	153 ± 32	172 ± 18	0.33 ± 0.10	40.2 ± 1.7	16 ± 4
	14.1		0.15	156 ± 38	153 ± 17	0.36 ± 0.09	38.2 ± 1.4	22 ± 4
	14.1		0.20	146 ± 34	146 ± 26	0.32 ± 0.07	34.1 ± 2.1	33 ± 4
	30.5			157 ± 28	148 ± 24	0.25 ± 0.02	33.8 ± 3.0	31 ± 4
	51.1			167 ± 32	156 ± 11	0.25 ± 0.01	31.9 ± 0.6	27 ± 3
	14.1		0.30	289 ± 23	241 ± 14	0.31 ± 0.03	31.1 ± 1.4	45 ± 7
	14.1	1.50	0.20	167 ± 31	167 ± 16	0.31 ± 0.07	32.4 ± 2.0	28 ± 3
	14.1	2.00	0.20	218 ± 17	171 ± 15	0.35 ± 0.05	33.7 ± 1.8	34 ± 3
	14.1	2.50	0.20	324 ± 25	192 ± 17	0.27± 0.12	36.3 ± 1.3	36 ± 4

285

286 The stability of polysaccharide nanoparticulate suspensions was studied at various pH
287 values in the range 3 to 8.5, with the main results being summarised in *Figure 2*. PUL-OX4
288 nanoparticles demonstrated better stability compared to the other materials under investigation,
289 showing only a slight increase in size; the diameter remained always below 200 nm, as the
290 modified pullulan was unaffected by pH changes due to the absence of ionisable groups
291 (Barbosa, Abdelsadig, Conway, & Merchant, 2019). For GG-OX4 nanoparticles, an increase
292 in size and a decrease in zeta potential were noticed at pH ≤4, where acidic conditions likely
293 catalysed additional intermolecular cross-linking between the existing hemiacetals and the
294 hydroxyl groups present on neighbouring macromolecules, leading eventually to
295 agglomeration (Hongbo, Yanping, Wen, & Siqing, 2016; Pal, Paulson, & Rousseau, 2009).
296 Freshly formulated CS-OX4 nanoparticles were cationic (with zeta potential around + 30 mV),
297 and showed a stable diameter in acidic conditions (ca. 140 nm). However, as the pH increased
298 above the pKa value of chitosan (ca. 6.3 (Wang et al., 2006)), a significant augmentation in
299 diameter accompanied by a noticeable loss of stability (resulting from the deprotonation of the
300 amine groups in chitosan around the isoelectric point) were observed.
301

A)

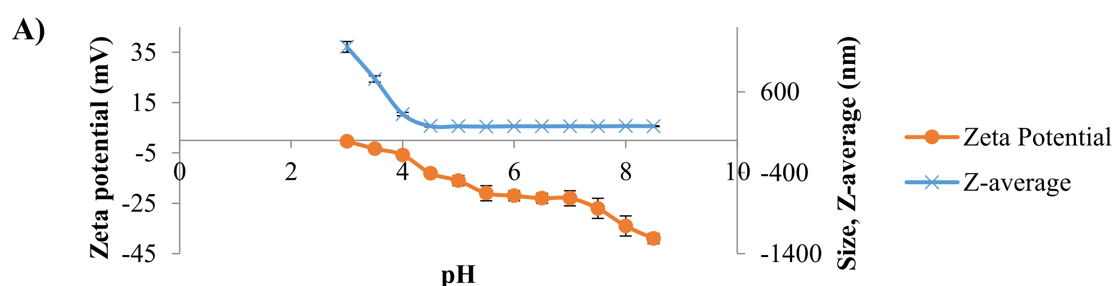

302

B)

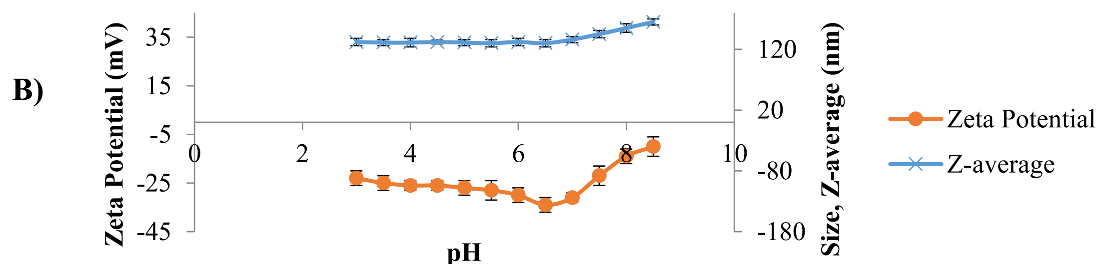

303

C)

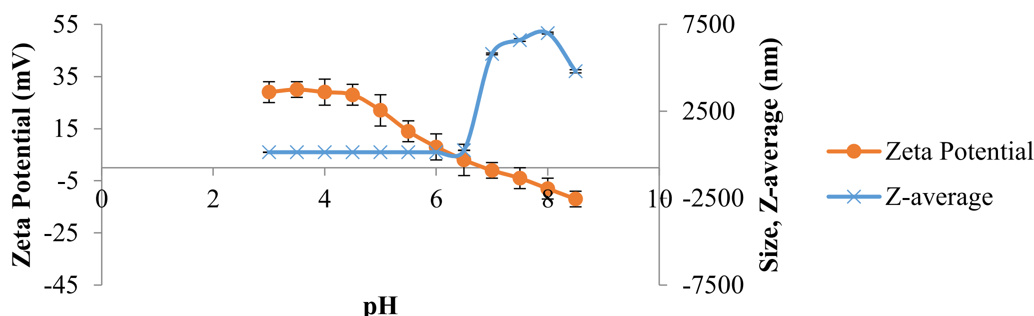

Figure 2. The influence of pH on the size and zeta potential of: A) GG-OX4, B) PUL-OX4, and C) CS-OX4 nanoparticles (1 mg/mL) (n=3, ±SD).

The nanoparticle morphology is exemplified in *Figure 3*. GG-OX4 and CS-OX4 nanoparticles were found to have the tendency to agglomerate during the purification and lyophilisation stages; the larger residual fragments visible in their SEM images (ribbon-like in Figure 3a, and fibre-like in Figure 3C) are attributed to the cross-linking reactions (with glutaraldehyde and sodium tripolyphosphate, respectively) employed during the formulation of these types of nanoparticles and drying during SEM sample preparation. PUL-OX4 nanoparticles showed a close to spherical morphology, in accordance with literature (Jung, Jeong, Kim, & Kim, 2004). SEM image indicated the CS-OX4 NPs were packed together after centrifugation and lyophilisation, which also affected their morphology. TEM images for PUL-OX4 and CS-OX4 NPs confirmed their spherical-like shape.

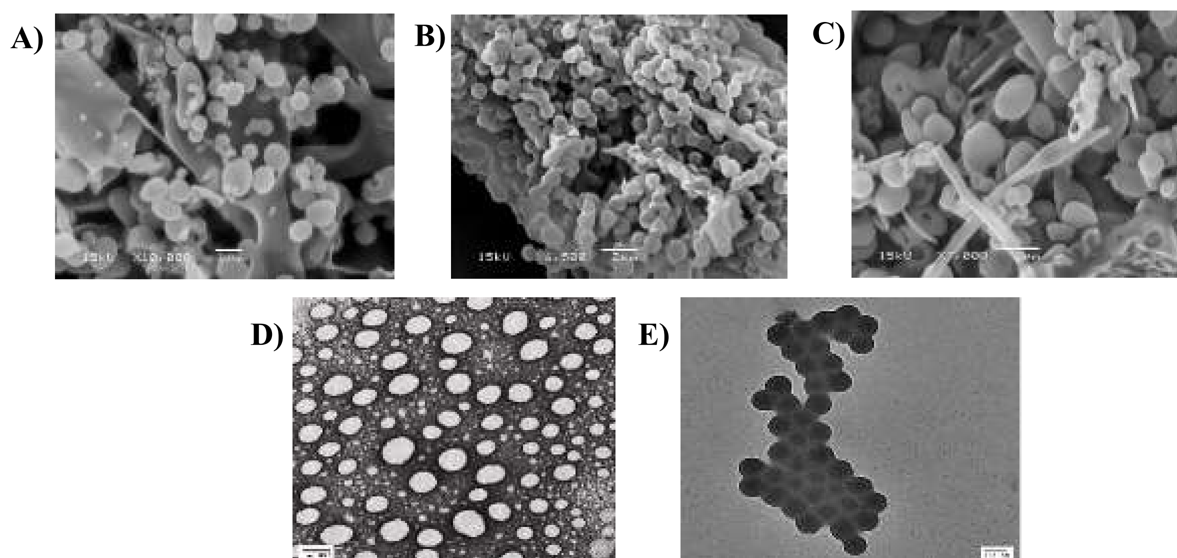

Figure 3. SEM micrograph of lyophilised nanoparticles: A) GG-OX4 (Bar: 1µm), B) PUL-OX4 (Bar: 2µm), C) CS-OX4 (Bar: 2µm), and TEM micrograph of nanoparticles from: D) PUL-OX4 (Bar: 100 nm, 2% uranyl acetate staining), and E) CS-OX4 (Bar: 100 nm, 2% uranyl acetate staining).

325

326 In order to monitor their fate *in vitro*, nanoparticles were fluorescently labelled using
327 either Texas Red-X dichlorotriazine (for GG-OX4 and PUL-OX4) or Texas Red-X
328 succinimidyl ester (for CS-OX4). The degree of labelling was determined as follows: 1.84% ±
329 0.51 for CS-OX4, 5.51% ± 1.29 for PUL-OX4, and 11.98% ± 2.56 for GG-OX4 (n=3, ±SD).
330 CS-OX4 showed the lowest degree of labelling, likely due to the heterogeneous nature of the
331 reaction (Sadki, 2011), which was carried out in suspension.

332 Model actives (MW 500-1000 Da, BCS class III or peptides (Benival & Devarajan,
333 2015; Volpe, 2004)) such as Doxorubicin and Rhodamine B that are known to be effluxed (Lee
334 et al., 1994), and Angiotensin II were employed to investigate the drug loading and drug release
335 profiles in/from the carriers. GG-OX4 nanoparticles exhibited the highest loading for
336 Rhodamine B (3.78% ± 0.6) and Doxorubicin (19.11% ± 1.2), while Angiotensin II showed
337 the highest load in PUL-OX4 (8.46% ± 1.0). Other results were presented as follows: CS-OX4
338 NPs had DL 1.38% ± 0.1, 3.56% ± 0.7, and 11.13% ± 1.6 for Rhodamine B, Angiotensin II
339 and Doxorubicin respectively; GG-OX4 exhibited DL 6.11% ± 1.2 for Angiotensin II; and
340 PUL-OX4 showed DL 2.11% ± 0.1 and 6.13% ± 0.8 for Rhodamine B and Doxorubicin
341 respectively (n=3, ±SD). Overall, nanoparticles with negative zeta potential (GG-OX4 and
342 PUL-OX4) demonstrated higher loading for positively-charged actives (Rhodamine B and
343 Doxorubicin (Janes, Fresneau, Marazuela, Fabra, & Alonso, 2001; Selvam et al., 2008);
344 Angiotensin II net charge +1.4) compared to CS-OX4 (with the only exception of
345 Doxorubicin). The covalent cross-linking of GG-OX4 NPs with glutaraldehyde is likely to have
346 contributed positively to their good loading degree performance (George, Shah, & Shrivastav,
347 2019) when compared to the other two modified polysaccharides.

348 A similar release profile was observed for all types of nanoparticles *(Figure 4)*, where
349 an initial burst was followed by a plateau; this can be explained by the rapid release of the drug
350 adsorbed on the surface (Fu & Kao, 2010; Ottenbrite & Kim, 2000) and the porous structure
351 of the polymer matrix resulted from the lyophilisation. Interestingly, a delayed release of
352 almost 1 h and a very slow release afterwards were observed in all cases for Doxorubicin,
353 possibly because of a combined effect of a lower drug solubility in the saline employed as
354 release medium and stronger drug interactions with the matrix (especially for cross-linked
355 nanoparticles obtained from GG-OX4 and CS-OX4).

356

357

358

359

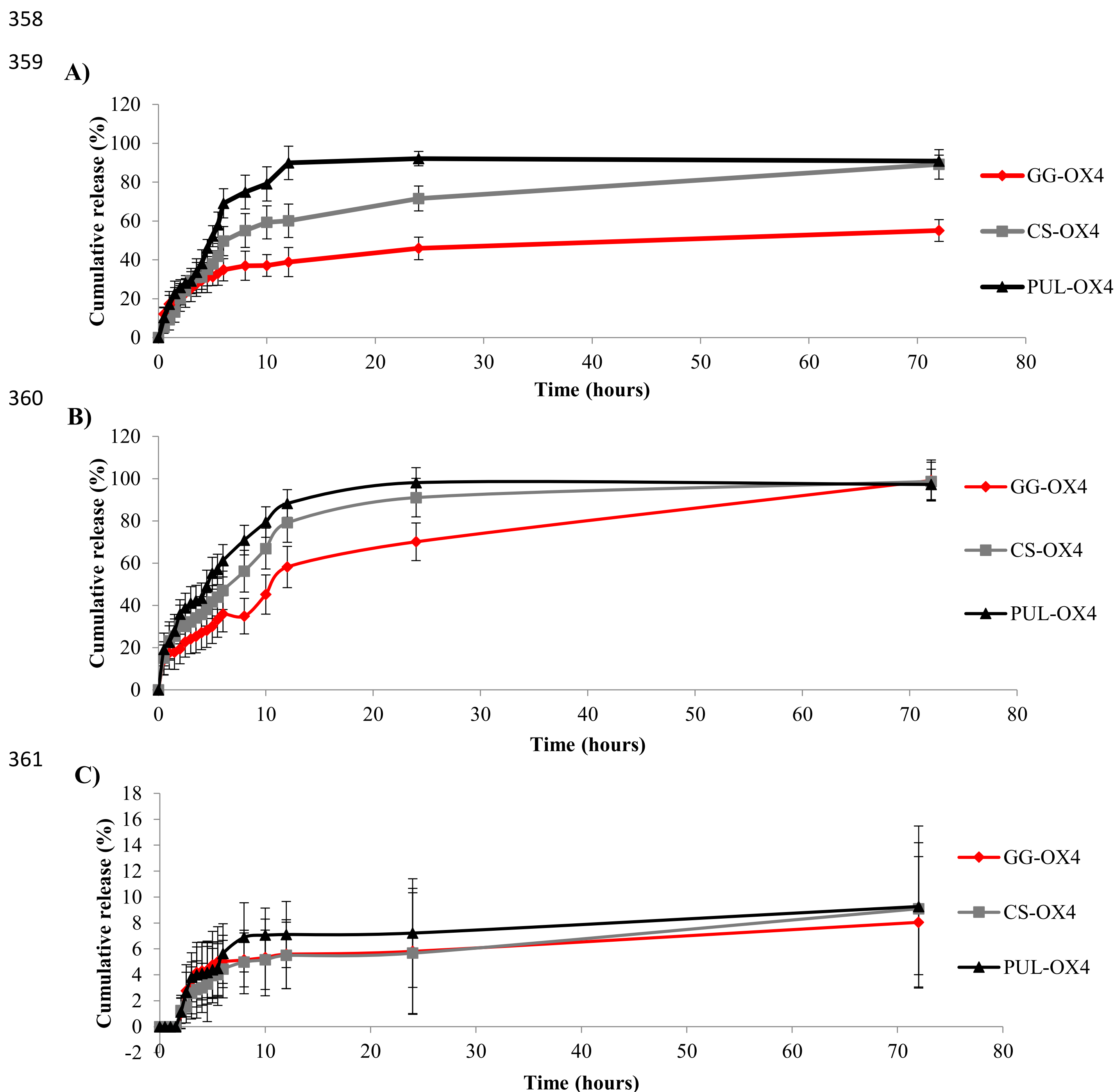

360

361

362

363 *Figure 4. Release profiles of: A) Rhodamine B, B) Angiotensin II, C) Doxorubicin from loaded*
364 *nanoparticles (1 mg/ml) in PBS (pH 7.4; saline 0.9%) (n=3, ±SD).*

365

366 The obtained drug release data were fitted in Higuchi, Hixon-Crowell and Korsmeyer-
367 Peppas kinetic models, and the quality of the fit was evaluated using the squared correlation
368 coefficient (R^2). Doxorubicin release was found to be well described by the Korsmeyer-Peppas
369 model, which indicated it is controlled by Fickian diffusion ($n < 0.5$), in contrast to the slow-
370 release behaviour mentioned in literature for Doxorubicin loaded into chitosan-stearic acid

371 micelles (Xie, Du, Yuan, & Hu, 2012). Angiotensin II release from GG-OX4 and PUL-OX4
372 NPs can be well described by the Higuchi's model, and it was found to be controlled only by
373 drug diffusion. For CS-OX4 NPs, the best fit was found with the Korsmeyer-Peppas model,
374 which indicated the release was controlled by non-Fickian transport ($n > 0.5$), possibly through
375 a combination of swelling and diffusion controlled release (Gulati, Nagaich, & Saraf, 2013).
376 The Korsmeyer-Peppas model was the best fit for Rhodamine B release from GG-OX4 ($n <$
377 0.5; Fickian diffusion), CS-OX4 ($n > 0.5$; non-Fickian diffusion), and PUL-OX4 NPs ($n > 1$;
378 super case II transport involving matrix swelling (Sahoo, Chakraborti, & Behera, 2012)).

379 An MTT assay was employed to study cytotoxicity of nanoparticles at different
380 concentrations (1–10 mg/mL), using PBS and Triton-X (0.1% v/v) as controls. The results
381 (*Figure 5)* showed that for application relevant concentrations (< 2 mg/mL) the cytotoxicity
382 was not significant compared to the PBS control, where nanoparticles showed 85% cell
383 viability. An increased cytotoxicity was observed however at higher concentrations (≥ 4
384 mg/mL), where the cell viability decreased below 75%, similar to the results reported for
385 nanoparticles prepared from dextran modified with alkylglycidyl ether (Toman et al., 2015).

386 The LC_{50} (lethal concentration 50) on bEnd3 cells was determined, it was found that
387 PUL-OX4 NPs exhibited the lowest toxicity (LC_{50} 9.48 ±0.98 mg/mL), followed by GG-OX4
388 (LC_{50} 8.84 ±0.76 mg/mL), with CS-OX4 showing the highest toxicity (LC_{50} 7.30 ±0.77
389 mg/mL).
390

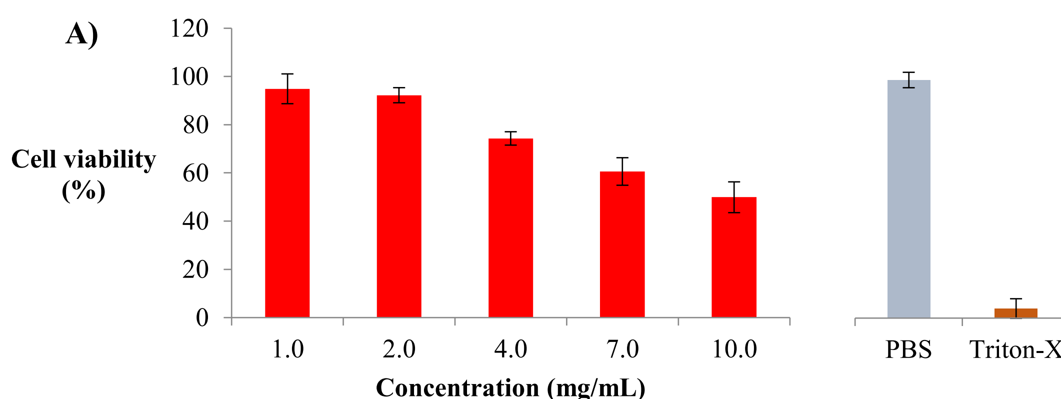

391

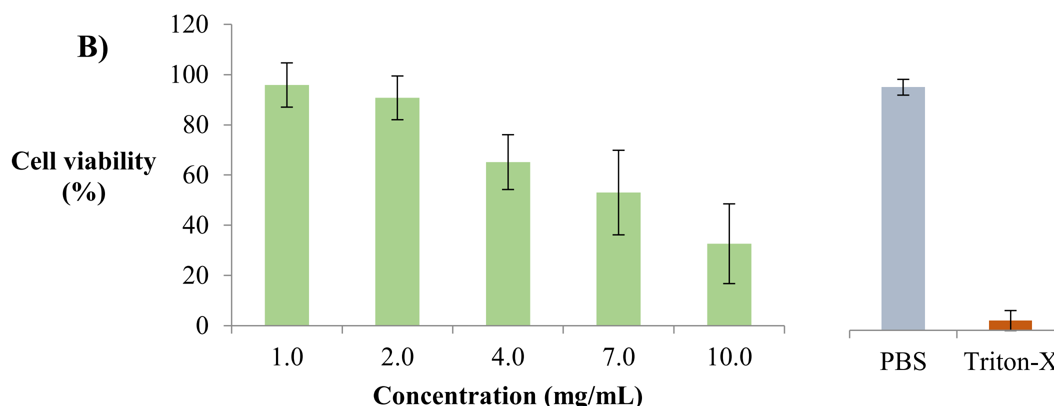

392

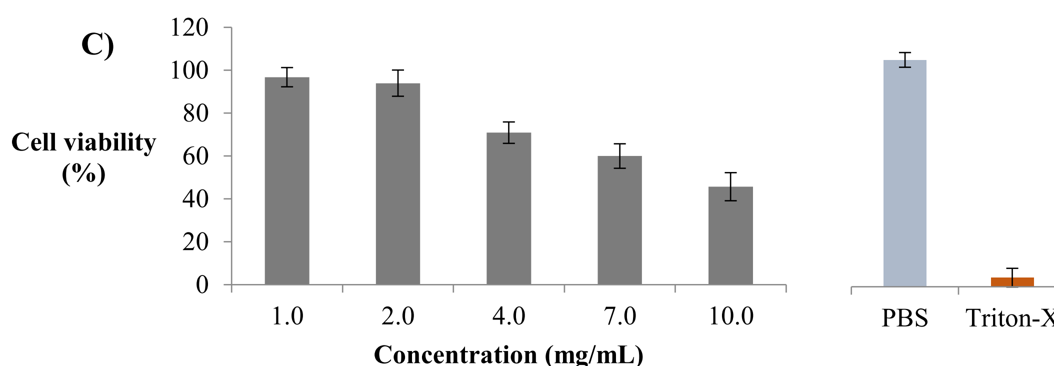

393

394 *Figure 5. Nanoparticles relative cytotoxicity against bEnd3 cells: A) PUL-OX4, B) CS-OX4,*
395 *and C) GG-OX4. bEnd3 cells incubated with nanoparticles (1–10 mg/mL); PBS and Triton-X*
396 *(0.1% v/v) as controls (n=36, ±SD).*
397

398 The interactions of nanoparticles with bEnd3 cells was investigated further using
399 confocal microscopy and employing Texas Red-labelled nanoparticles (*Figure 6*). Results
400 suggest the NPs were taken up by cells and localised in the cytoplasm, appearing not to enter
401 the nucleus), as previously found with butylglyceryl-modified chitosan nanoparticles (Lien et
402 al., 2012); the uptake is suggested as being triggered *via* caveolar/clathrin-mediated
403 endocytosis (Petros & DeSimone, 2010). Aggregation of nanoparticles outside cells and at the
404 interface with the cell membranes was observed for CS-OX4, due to a lower stability of CS-
405 OX4 formulations at pH 7.4 combined with the effect of the interactions between positively-
406 charged nanoparticles and negatively-charged cell membrane.
407 Results obtained from flow cytometry recorded a higher than 85% uptake. PUL-OX4
408 nanoparticles (99.32%) exhibited the highest and CS-OX4 showed the lowest (87.88%; likely
409 because of nanoparticles clustering, evidenced by the stability and confocal microscopy
410 results), while GG-OX4 also exhibited a relatively high uptake with 95.25%.

411

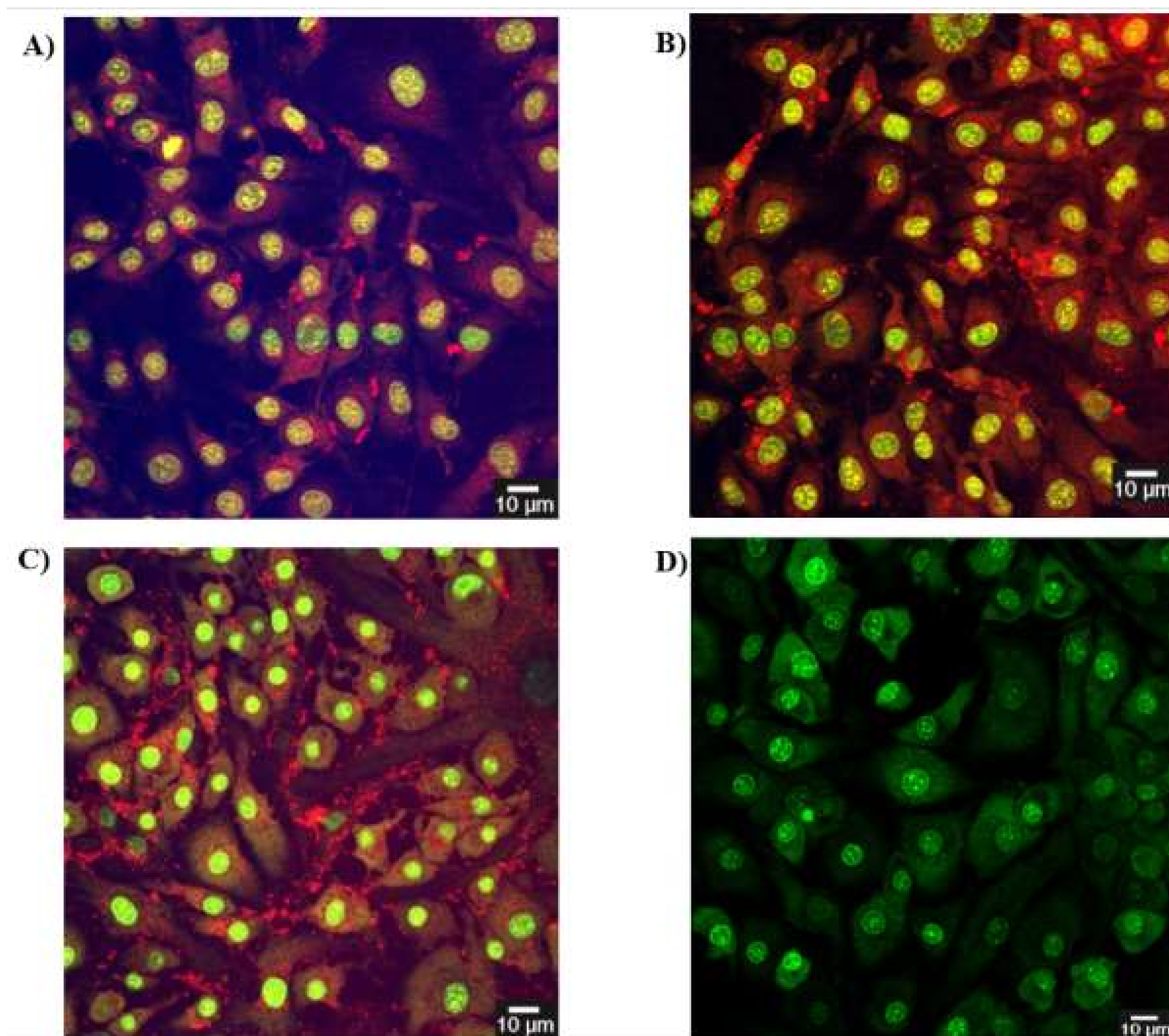

412

413 *Figure 6. Confocal microscope images of bEnd3 cells treated with Texas Red-labelled*
414 *nanoparticles (in red) from: A) PUL-OX4, B) GG-OX4, and C) CS-OX against black*
415 *background. bEnd3 cells treated with NucGreen Dead 488 (in green; without nanoparticles)*
416 *was used as a control (D) – Bar: 10 μm.*

417

418

419 The effect on bEnd3 cells permeability was investigated using a Transwell-type BBB
420 model comprising of a confluent bEnd3 cells monolayer enriched with a barrier enhancing
421 formula (Lien et al., 2012); FITC-dextran (500 kDa) as a fluorescent marker. The longer the
422 incubation time, the higher the permeability as noted for CS-OX4 and PUL-OX4 showing a
423 significant effect after 3 h (*Figure 7),* in contrast to GG-OX4.

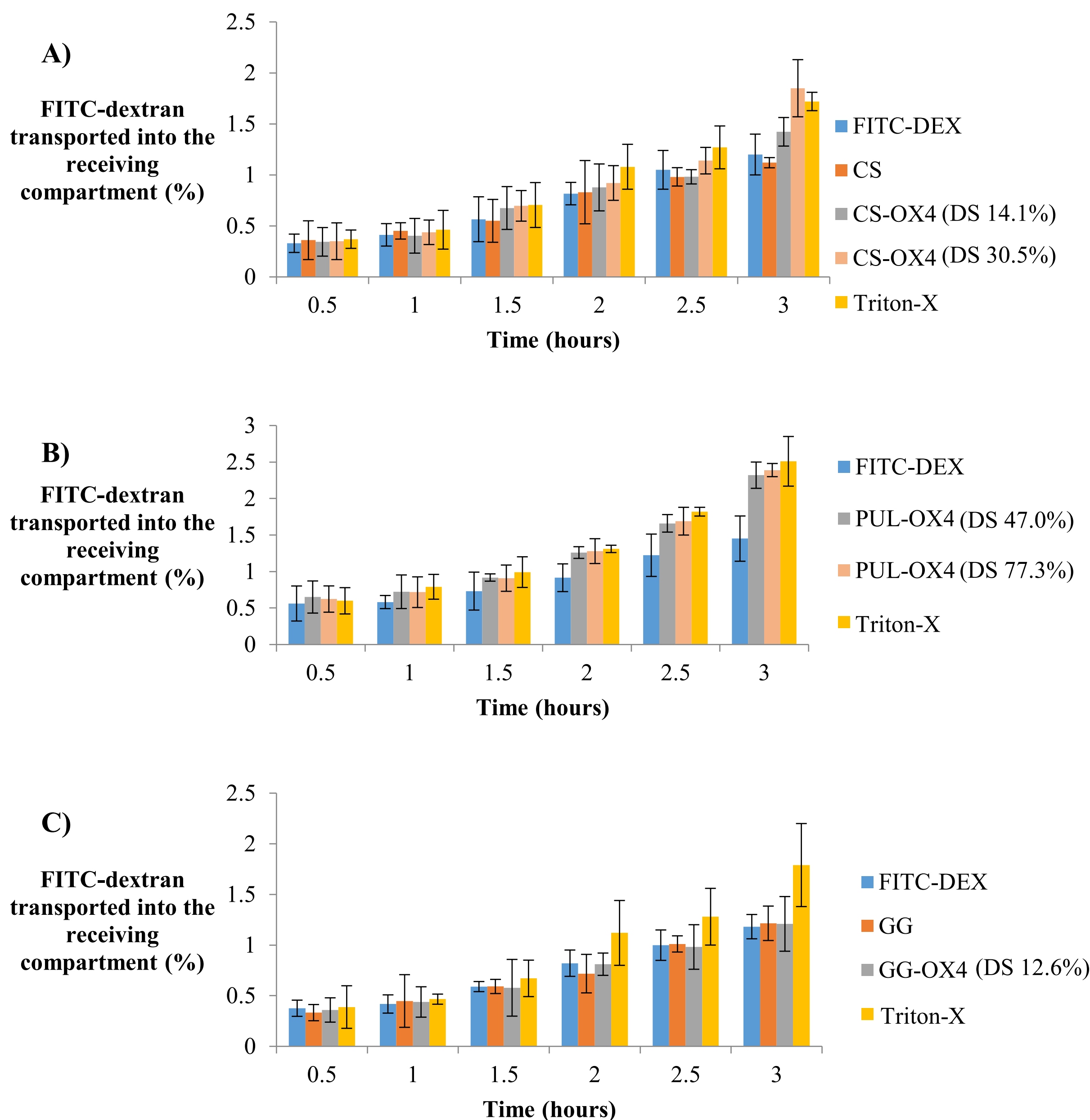

Figure 7. FITC-DEX translocation through bEnd3 cell monolayers following treatment with nanoparticles (2 mg/mL) prepared from either native polysaccharides or butylglyceryl-modified polysaccharide: A) CS-OX4, B) PUL-OX4, and C) GG-OX4. FITC-dextran and Triton-X (0.2 %) were employed as controls (n=5, ±SD).

The results of permeability studies (summarised in *Table 2)* indicated that the FITC-dextran paracellular transport across the bEnd3 monolayer increased with the DS; PUL-OX4 (DS 77.3%) showed the highest permeability enhancing effect (P_{app} value of 5.64 x 10^{-5} at 3 h); this value is higher than previously reported for alkylglyceryl-modified dextran with DS 130–142%; (1.5–1.6 x 10^{-7}; (Toman et al., 2015). No significant toxicity was induced at the concentration of 2 mg/mL, therefore it was assumed the translocation is not related to any

438 model membrane leaks associated with cell death. A concentration dependent effect was
439 observed, however the trend was inconsistent for GG-OX4 (possibly because of the low DS of
440 GG-OX4 used).

441

442

443 *Table 2. Permeability coefficients (P_{app}) calculated from experiments using mouse bEnd3 cells*
444 *treated with nanoparticles (2 mg/mL) at 3 h incubation time. FITC-DEX and Triton-X as*
445 *controls (n=5, ±SD).*

Material	Degree of substitution (%)	Concentration	P_{app} 3 hours
FITC-DEX	-	100 µg/mL	(3.28 ± 0.09) x 10^{-5}
CS	0	2.0 mg/mL	(3.21 ± 0.04) x 10^{-5}
CS-OX4	14.1	0.5 mg/mL	(3.55 ± 0.14) x 10^{-5}
	30.5	0.5 mg/mL	(4.11 ± 0.25) x 10^{-5}
		2.0 mg/mL	(4.94 ± 0.28) x 10^{-5}
PUL-OX4	47.0	2.0 mg/mL	(4.55 ± 0.19) x 10^{-5}
	77.3	0.5 mg/mL	(4.64 ± 0.13) x 10^{-5}
		2.0 mg/mL	(5.64 ± 0.09) x 10^{-5}
GG	0	2.0 mg/mL	(3.38 ± 0.20) x 10^{-5}
GG-OX4	12.6	0.5 mg/mL	(3.36 ± 0.23) x 10^{-5}
		2.0 mg/mL	(3.56 ± 0.18) x 10^{-5}
Triton-X	-	0.2 % v/v	(6.97 ± 0.33) x 10^{-5}

446

447

448 Rationalised by the fact that most of the therapeutic applications are intravenous-based,
449 a haemolysis study was performed in order to investigate the potential toxicity of nanoparticles
450 towards red blood cells, RBC (*Figure 8)*; the NP concentration effect on the RBC lysis was
451 also studied. Results indicated no toxicity at concentrations below 12 mg/mL, showing less
452 than 10% haemolysis compared to the PBS control. A certain degree of haemolysis was found
453 however with increasing the concentration further, and calculated LC_{30} values (19.87 mg/mL,
454 18.01 mg/mL, and 13.95 mg/mL for PUL-OX4, GG-OX4, and CS-OX4, respectively)
455 indicated that PUL-based NPs exhibit the least haemolytic effect. In contrast, at high
456 concentrations, CS-OX4 nanoparticles were found to induce the strongest haemolytic effect,
457 likely due to interactions between positively-charged chitosan and negatively-charged cell
458 membranes leading to membrane damage (Narayanan, Anitha, Jayakumar, Nair, & Chennazhi,
459 2012).

460

461

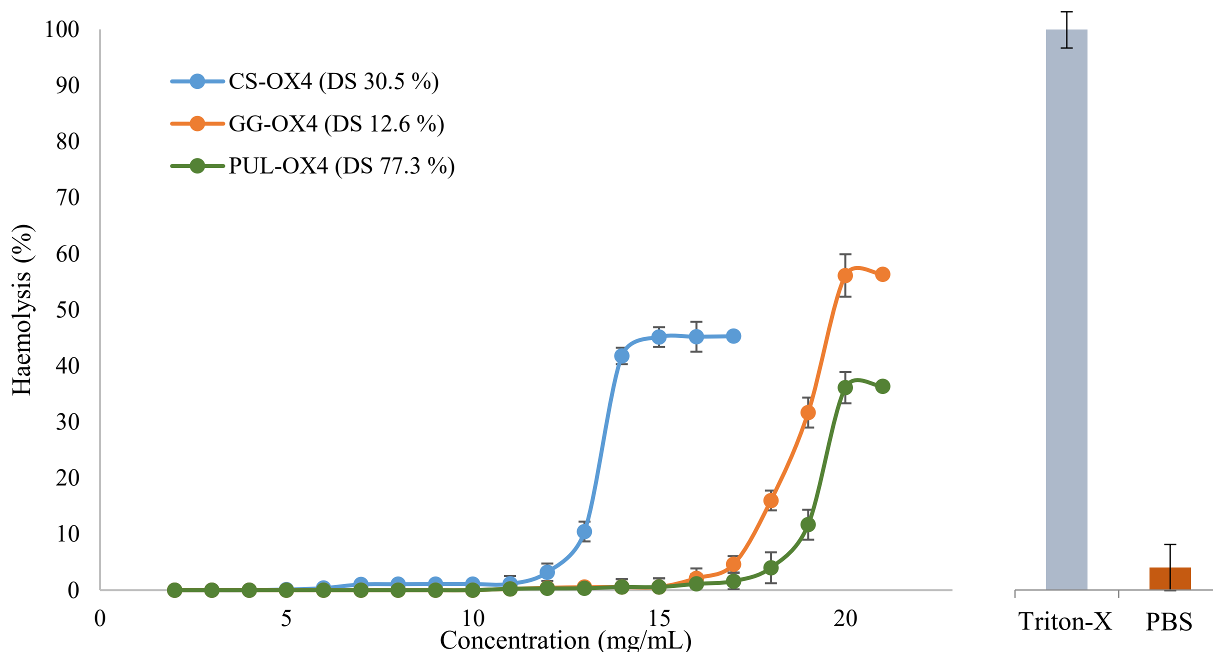

462
463 *Figure 8. Haemolysis test results using rat RBC exposed to butylglyceryl-modified*
464 *nanoparticles of varying concentrations. RBC suspension mixed with PBS or Triton-X (1%)*
465 *were used as controls (n=3; ±SD).*
466
467
468 **4. Conclusions**
469
470 Amphiphilic butylglyceryl derivatives of guar gum, pullulan, and chitosan (prepared
471 *via* modification with *n*-butylglycidyl ether) can be formulated using various methods into
472 nanogels (120–200 nm diameter) to be employed as drug carriers. However, only PUL-OX4
473 colloidal formulations demonstrated acceptable stability over the whole range of pH tested (3
474 - 8.5).
475 GG-OX4 NPs showed the highest loading capacity for high molecular weight model
476 actives that are known to be effluxed (such as Rhodamine B and Doxorubicin), while PUL-
477 OX4 NPs were found to perform better for high molecular weight and hydrophilic
478 biomacromolecules such as Angiotensin II peptide; the drug release profiles can be best
479 described by either Korsmeyer-Peppas or Higuchi equations, and showed in all cases an initial
480 burst discharge followed by a gradual release phase.
481 PUL-OX4 NPs demonstrated the lowest cytotoxicity (i.e. highest LC_{50} value, as
482 determined by MTT) and the weakest haemolytic effect. All NPs were taken up by bEnd3 brain
483 endothelial cells, with PUL-OX4 NPs showing the highest uptake. The presence of
484 butylglyceryl-modified nanoparticles enhanced the FITC-DEX transport across the bEnd3-

485 based BBB model membranes, with PUL-OX4 nanoparticles showing the highest drug
486 permeability enhancing effect. Overall, our results suggest that PUL-OX4 nanoparticles would
487 warrant further development as they demonstrate most promising characteristics for potential
488 use in brain drug delivery applications.
489

490 Acknowledgements

491 This study was supported by the Majlis Amanah Rakyat (Malaysia), University of
492 Portsmouth (UK), and Al Ain University (UAE).

493

494 **References**

495 Barbosa, J. A. C., Abdelsadig, M. S. E., Conway, B. R., & Merchant, H. A. (2019). Using zeta potential
496 to study the ionisation behaviour of polymers employed in modified-release dosage forms
497 and estimating their pKa. *International journal of pharmaceutics: X, 1*, 100024.
498 Benival, D. M., & Devarajan, P. V. (2015). In situ lipidization as a new approach for the design of a self
499 microemulsifying drug delivery system (SMEDDS) of doxorubicin hydrochloride for oral
500 administration. *Journal of biomedical nanotechnology, 11*(5), 913-922.
501 Bostanudin, M. F., Arafat, M., Sarfraz, M., Górecki, D. C., & Barbu, E. (2019). Butylglyceryl pectin
502 nanoparticles: synthesis, formulation and characterization. *Polymers, 11*(5), 789.
503 Boussahel, A., Ibegbu, D. M., Lamtahri, R., Maucotel, J., Chuquet, J., Lefranc, B., . . . Gorecki, D.
504 (2017). Investigations of octylglyceryl dextran-graft-poly (lactic acid) nanoparticles for
505 peptide delivery to the brain. *Nanomedicine, 12*(8), 879-892.
506 Chen, Y., Mohanraj, V. J., Wang, F., & Benson, H. A. E. (2007). Designing chitosan-dextran sulfate
507 nanoparticles using charge ratios. *AAPS PharmSciTech, 8*(4), 131-139.
508 Erdlenbruch, B., Schinkhof, C., Kugler, W., Heinemann, D. E. H., Herms, J., Eibl, H., & Lakomek, M.
509 (2003). Intracarotid administration of short-chain alkylglycerols for increased delivery of
510 methotrexate to the rat brain. *British journal of pharmacology, 139*(4), 685-694.
511 Fu, Y., & Kao, W. J. (2010). Drug release kinetics and transport mechanisms of non-degradable and
512 degradable polymeric delivery systems. *Expert opinion on drug delivery, 7*(4), 429-444.
513 George, A., Shah, P. A., & Shrivastav, P. S. (2019). Guar gum: Versatile natural polymer for drug
514 delivery applications. *European Polymer Journal, 112*, 722-735.
515 Godfrey, L., Iannitelli, A., Garrett, N. L., Moger, J., Imbert, I., King, T., . . . Schätzlein, A. G. (2018).
516 Nanoparticulate peptide delivery exclusively to the brain produces tolerance free analgesia.
517 *Journal of controlled release, 270*, 135-144.
518 Gulati, N., Nagaich, U., & Saraf, S. A. (2013). Intranasal delivery of chitosan nanoparticles for
519 migraine therapy. *Scientia pharmaceutica, 81*(3), 843.
520 Hervé, F., Ghinea, N., & Scherrmann, J.-M. (2008). CNS delivery via adsorptive transcytosis. *The AAPS
521 journal, 10*(3), 455-472.
522 Hongbo, T., Yanping, L., Wen, Z., & Siqing, D. (2016). Synthesis, optimization, property,
523 characterization, and application of dialdehyde cross-linking guar gum. *International Journal
524 of Polymer Science, 2016*.
525 Ibegbu, D. M., Boussahel, A., Cragg, S. M., Tsibouklis, J., & Barbu, E. (2017). Nanoparticles of
526 alkylglyceryl dextran and poly (ethyl cyanoacrylate) for applications in drug delivery:
527 Preparation and characterization. *International Journal of Polymeric Materials and Polymeric
528 Biomaterials, 66*(6), 265-279.
529 Janes, K. A., Fresneau, M. P., Marazuela, A., Fabra, A., & Alonso, M. a. J. (2001). Chitosan
530 nanoparticles as delivery systems for doxorubicin. *Journal of controlled Release, 73*(2-3),
531 255-267.
532 Jung, S.-W., Jeong, Y.-I., Kim, Y.-H., & Kim, S.-H. (2004). Self-assembled polymeric nanoparticles of
533 poly (ethylene glycol) grafted pullulan acetate as a novel drug carrier. *Archives of pharmacal
534 research, 27*(5), 562-569.
535 Lalatsa, A., & Barbu, E. (2016). Carbohydrate nanoparticles for brain delivery. In *International review
536 of neurobiology* (Vol. 130, pp. 115-153): Elsevier.
537 Lalatsa, A., Schatzlein, A. G., & Uchegbu, I. F. (2014). Strategies to deliver peptide drugs to the brain.
538 *Molecular pharmaceutics, 11*(4), 1081-1093.
539 Lalatsa, A., Schätzlein, A. G., Garrett, N. L., Moger, J., Briggs, M., Godfrey, L., . . . Uchegbu, I. F.
540 (2015). Chitosan amphiphile coating of peptide nanofibres reduces liver uptake and delivers
541 the peptide to the brain on intravenous administration. *Journal of Controlled Release, 197*,
542 87-96.

543 Lee, J.-S., Paull, K., Alvarez, M., Hose, C., Monks, A., Grever, M., . . . Bates, S. E. (1994). Rhodamine
544 efflux patterns predict P-glycoprotein substrates in the National Cancer Institute drug
545 screen. *Molecular pharmacology, 46*(4), 627-638.
546 Lien, C.-F., Molnár, E. v., Toman, P., Tsibouklis, J., Pilkington, G. J., Górecki, D. C., & Barbu, E. (2012).
547 In vitro assessment of alkylglyceryl-functionalized chitosan nanoparticles as permeating
548 vectors for the blood–brain barrier. *Biomacromolecules, 13*(4), 1067-1073.
549 Lu, C.-T., Zhao, Y.-Z., Wong, H. L., Cai, J., Peng, L., & Tian, X.-Q. (2014). Current approaches to
550 enhance CNS delivery of drugs across the brain barriers. *International journal of*
551 *nanomedicine, 9*, 2241.
552 Molnár, E. v., Barbu, E., Lien, C.-F., Górecki, D. C., & Tsibouklis, J. (2010). Toward drug delivery into
553 the brain: synthesis, characterization, and preliminary in vitro assessment of alkylglyceryl-
554 functionalized chitosan nanoparticles. *Biomacromolecules, 11*(11), 2880-2889.
555 Narayanan, D., Anitha, A., Jayakumar, R., Nair, S. V., & Chennazhi, K. P. (2012). Synthesis,
556 characterization and preliminary in vitro evaluation of PTH 1-34 loaded chitosan
557 nanoparticles for osteoporosis. *Journal of biomedical nanotechnology, 8*(1), 98-106.
558 Ottenbrite, R. M., & Kim, S. W. (2000). *Polymeric drugs and drug delivery systems*: CRC Press.
559 Pal, K., Paulson, A. T., & Rousseau, D. (2009). Biopolymers in controlled-release delivery systems. In
560 *Modern biopolymer science* (pp. 519-557): Elsevier.
561 Petros, R. A., & DeSimone, J. M. (2010). Strategies in the design of nanoparticles for therapeutic
562 applications. *Nature reviews Drug discovery, 9*(8), 615-627.
563 Raggi, A., & Leonardi, M. (2019). Burden of brain disorders in Europe in 2017 and comparison with
564 other non-communicable disease groups. *Journal of Neurology, Neurosurgery & Psychiatry*,
565 jnnp-2019.
566 Sadki, M. S. (2011). Hydrophobically modified derivatives of polysaccharides.
567 Sahoo, S., Chakraborti, C. K., & Behera, P. K. (2012). Development and evaluation of gastroretentive
568 controlled release polymeric suspensions containing ciprofloxacin and carbopol polymers. *J*
569 *Chem Pharm Res, 4*, 2268-2284.
570 Selvam, P. P., Preethi, S., Basakaralingam, P., Thinakaran, N., Sivasamy, A., & Sivanesan, S. (2008).
571 Removal of rhodamine B from aqueous solution by adsorption onto sodium
572 montmorillonite. *Journal of Hazardous Materials, 155*(1-2), 39-44.
573 Singh, R. S., Kaur, N., Rana, V., & Kennedy, J. F. (2017). Pullulan: a novel molecule for biomedical
574 applications. *Carbohydrate polymers, 171*, 102-121.
575 Toman, P., Lien, C.-F., Ahmad, Z., Dietrich, S., Smith, J. R., An, Q., . . . Tsibouklis, J. (2015).
576 Nanoparticles of alkylglyceryl-dextran-graft-poly (lactic acid) for drug delivery to the brain:
577 Preparation and in vitro investigation. *Acta biomaterialia, 23*, 250-262.
578 Volpe, D. A. (2004). Permeability classification of representative fluoroquinolones by a cell culture
579 method. *AAPS PharmSci, 6*(2), 1-6.
580 Wang, Q. Z., Chen, X. G., Liu, N., Wang, S. X., Liu, C. S., Meng, X. H., & Liu, C. G. (2006). Protonation
581 constants of chitosan with different molecular weight and degree of deacetylation.
582 *Carbohydrate polymers, 65*(2), 194-201.
583 Xie, Y.-T., Du, Y.-Z., Yuan, H., & Hu, F.-Q. (2012). Brain-targeting study of stearic acid–grafted
584 chitosan micelle drug-delivery system. *International journal of nanomedicine, 7*, 3235.

585